Proceedings of the ASME 2010 3rd Joint US-European Fluids Engineering Summer Meeting and 8th International Conference on Nanochannels, Microchannels, and Minichannels
FEDSM-ICNMM2010
August 1-5, 2010, Montreal, Canada

FEDSM-ICNMM2010-30074

FLOW CONDITIONS AT THE INLET OF ASPIRATING PIPES: PART 1 - THEORY

François Axisa
Visiting researcher at ITN/ADL
Paris, France

ABSTRACT

Drastic changes occur in the dynamics of pipes conveying fluid when passing from the discharging flow case to the aspirating flow case. This can be attributed to modifications in the flow conditions which prevail at the aspirating tube inlet versus those prevailing at a discharging tube outlet. In the present paper the point is investigated in relation with the behavior of two elementary systems, namely a single degree of freedom system (1-DOF oscillator) made of a rigid pipe supported at one end by a rotational spring and a two degrees of freedom system (2-DOF coupled oscillators) made of a pair of articulated tubes. In the first system, flow-structure coupling reduces essentially to a Coriolis force while in the second, it arises via both centrifugal and Coriolis forces. The present paper is devoted to theoretical modeling and prediction of the dynamical behavior of these systems according to a few basic assumptions concerning the flow conditions at the aspirating inlet. It serves as an introduction to the companion paper by Debut et al. [1] where theoretical predictions are confronted to experiment. As a major result it is found that even "small changes" in the flow conditions at the aspirating inlet can lead to important changes in the tube dynamics which are amenable to measurement, even if the experiments are restricted to relatively low flow velocities because of limited capacity of the test loop.

1 INTRODUCTION

Since about two decades it was recognized that the dynamics of cantilevered pipes conveying fluid drastically differs depending whether the fluid discharges freely into the atmosphere, or equivalently into a large volume of liquid, at the free end of the pipe, or in the opposite case it is aspirated from it, see Hsu [2], Païdoussis [3-7] Kuiper & Metrikine [8-10], Giacobbi et al.[11,12]. Briefly summarized, in discharging flow, linear instability of the pipe via 1-DOF flutter is observed beyond a certain critical value of mean flow velocity. Moreover, the critical value at which flutter is initiated may be satisfactorily predicted based on a flow-structure coupling mechanism which is linear in nature and entirely governed by the unsteady inertia force of the conveyed fluid, see in particular the comprehensive book by M.P. Païdoussis [3] which reviews exhaustively the research work devoted to the subject up to the nineties. In contrast, according to the experiments performed independently by Kuiper et al. at TNO Delft, and by Païdoussis and co-workers at McGill Montreal, in aspirating flow, the linear flutter instability has not been identified even if large vibrations can still be observed provided the flow velocity is high enough. According to these authors, they correspond to rather complicated and irregular sequences of large amplitude orbital oscillations interrupted by quasi-chaotic motions of less amplitude which are likely related to some flow nonlinearity. Keeping to the linear domain, a major part of the difference observed was attributed to a drastic change between the flow conditions which prevail at the free outlet of a discharging tube and those which prevail at the free inlet of an aspirating tube. In this respect, a linear model including several variants has been proposed in refs [4,5] and [8], which comprises a depressurization effect related to the singular pressure drop at the tube intake and an unsteady force related to an abrupt change in flow momentum at the tube aspirating end.

As crude representations of reality this type of one dimensional and linear models of aspirating flow at the tube intake may be, they however have the virtue of bringing out major effects which can be reasonably expected to hold, at sufficiently low aspirating flow velocity, at least. Moreover their imprint on the dynamical behavior of the pipe is amenable to experimental diagnosis as further demonstrated in this paper and in a companion paper by Debut et al. [1]. Our approach

consists in analyzing the modal properties of two articulated pipe systems, especially selected for their theoretical simplicity and practical feasibility, first in discharging flow and then in aspirating flow, to infer the flow-coupling forces acting on the system. As a first part, described here, a few distinct flow conditions are assumed at the free aspirating pipe inlet, and the consequences on the response properties of the pipes are investigated by theory. This work served as a guideline to conduct pertinent validation experiments and stands here as an introduction to the companion paper [1], which is devoted to the experimental part of the present investigation.

2 FLEXIBLE PIPES CONVEYING FLUID

2.1 Equation of motion and energy balance

For mathematical and experimental convenience the present work deals with articulated and rigid pipe elements, the case of flexible pipes is however briefly reviewed first in order to set the points treated here into a more general context where the pipes behave as slender flexed beams. The motion of the pipe is described using the Euler-Bernoulli equation loaded by the coupling force induced by the conveyed fluid:

$$EI\frac{\partial^4 Z}{\partial x^4}-\frac{\partial}{\partial x}\left(T\frac{\partial Z}{\partial x}\right)+C_s\frac{\partial Z}{\partial t}+m_s\frac{\partial^2 Z}{\partial t^2}=f_{\mathcal{W}}(x;t). \tag{1}$$

$Z(x;t)$ denotes the lateral displacement field. *EI* is the flexural rigidity of the pipe, C_s is the viscous damping coefficient used to account for dissipation in still fluid and $m_s=\rho_s S_s$ means solid mass per unit pipe length. $T(x)$ stands either for an axial prestress, due to gravity for instance, or for an axial follower force. Finally, $f_{\mathcal{W}}(x;t)$ is the net force per unit pipe length exerted in the direction of the lateral motion of the pipe wall by the internal flowing fluid. It comprises a few distinct components related to fluid inertia, pressure and viscous stresses. It turns out however that if the pressure field is entirely controlled by viscous losses (no pressurization), the resulting pressure force is exactly cancelled by the viscous stresses in such a manner that $f_{\mathcal{W}}(x;t)$ reduces to the inertia component. According to the plug-flow model which assumes a uniform steady flow velocity, it may be written as

$$\vec{f}^{\,I}_{\mathcal{W}}=-m_f\frac{D\vec{V}}{Dt}=-m_f\frac{D^2Z}{Dt^2}\vec{k}=-m_f\left(\frac{\partial}{\partial t}+V\frac{\partial}{\partial x}\right)^2 Z\vec{k}. \tag{2}$$

D/Dt denotes the material time derivative and $\vec{V}(x;t)$ is the Eulerian flow velocity field, which stands for an unsteady entity since the flow is perturbed by the motion of the tube. V denotes the mean flow velocity as averaged over the cross-sectional area of the tube. The mass of conveyed fluid per unit tube length is $m_f=\rho_f S_f$. The unit vector $\vec{k}$ indicates the direction of the lateral vibration. If the tube is pressurized by a uniform pressure P_p counted from the external ambient pressure, the force becomes:

$$\vec{f}_{\mathcal{W}}=\vec{f}^{\,I}_{\mathcal{W}}-S_f\frac{\partial\left(P_p\vec{\ell}\right)}{\partial x}=-m_f\left(\frac{\partial^2 Z}{\partial t^2}+2V\frac{\partial^2 Z}{\partial t\partial x}+\left(V^2+\frac{P_p}{\rho_f}\right)\frac{\partial^2 Z}{\partial x^2}\right), \tag{3}$$

where $\vec{\ell}$ means the unit vector in the axial direction of the deflected tube. It is recalled that the first term in $\vec{f}_{\mathcal{W}}$ which is independent of V means the added mass force also present in still fluid, while the term proportional to V stands for a flow-induced Coriolis force, and the term proportional to V^2 means a flow-induced centrifugal force. Finally, the pressurization term is similar to the centrifugal force. Conservative or nonconservative nature of these forces depends on the support conditions at the pipe ends as can be conveniently discussed starting from the work done by the flow-structure coupling force on the whole tube of length L over a given time T. Using a few standard manipulations it is written as

$$\mathcal{W}_V(T)=-\int_0^T\left[m_fV\left(\frac{\partial Z}{\partial t}\right)^2+\left(m_fV^2+\frac{P_p}{\rho_f}\right)\frac{\partial Z}{\partial t}\frac{\partial Z}{\partial x}\right]_0^L dt$$
$$-\left(m_fV^2+\frac{P_p}{\rho_f}\right)\left[\left(X_L\right)\right]_0^T. \tag{4}$$

The last term in the above formula accounts for the work induced by the small change in the actual tube length induced by the lateral displacement. This change of length corresponds to the axial displacement:

$$X_L(t)=-\frac{1}{2}\int_0^L\left(\frac{\partial Z}{\partial x}\right)^2 dx \tag{5}$$

Considering first the contribution of the time integral solely, if $Z(0)=Z(L)=0$, no work is performed, neither by the Coriolis nor by the centrifugal force. As a consequence, periodic or damped vibration is expected depending on whether damping in still fluid is discarded, or not. Then, in the case of periodic motion, the contribution of the contraction term is nil, while in the damped case, it is negative since X_L decreases in magnitude with time proportionally to $\exp(-2\omega\varsigma t)$ where ω denotes the natural angular frequency of the vibration and ς the reduced damping. Nevertheless, in agreement with Done & Simpson [13], net energy can still be fed into the vibrating tube, even if lateral motion is prevented at both ends, provided the axial motion is not; which explains the post-divergence mechanism of coupled mode flutter discovered by Païdoussis & Issid [14]. The necessary work is related to the axial contraction of the pipe. This is the very reason why in the energy balance the last term is not dropped in contrast with the form broadly assumed in the open literature.

Finally, as soon as $Z(0)\neq Z(L)$ energy can be exchanged between the solid and the fluid due to the work of all terms in

the energy balance (5). Depending on its sign, the internal flow is found to damp out the vibration of the pipe or at the opposite to destabilize it via dynamic instability, commonly called 'flutter' for historical reasons related to the aeronautical industry, see Bisplinghoff et al. [15].

2.2 Flow conditions at the free tube end

The real flow conditions at a discharging pipe outlet largely differ from those which hold at an aspirating pipe inlet, in such a manner that more conditions than a sign change in mean flow velocity must be fulfilled to describe the mean flow properties when shifting from one operating mode to the other. A first mechanism to be considered is related to the steady pressure drop taking place at the end of the tube, which may be described using the concepts of pipe hydraulics. Accordingly, the steady pressure drop is assumed to be governed by the dissipative and steady version of Bernoulli's equation which reads as:

$$\left(\frac{1}{2}\rho_f \overline{V_1^2} + P_1\right) - \left(\frac{1}{2}\rho_f \overline{V_2^2} + P_2\right) = \Delta P_{\text{loss}} = \frac{1}{2}\rho_f V^2 K_{\text{loss}}, \tag{6}$$

where ΔP_{loss} means the pressure drop between two cross-sections, labelled (1) and (2) respectively. The overbar indicates that the dynamical pressure is averaged over the cross-sectional area. The corresponding mean flow velocity is again denoted by V for the sake of conciseness and $\overline{V_1^2} = \overline{V_2^2} = V^2$ is assumed to hold in agreement with the plug flow model. Finally, K_{loss} is the dimensionless coefficient of pressure loss. It is also worth recalling that equation (6) may be interpreted as an energy balance since it can be derived by integrating the energy equation between two cross-sections, under a few restrictive assumptions at least, see for instance Blevins [16]. As a well known result, if the flow discharges freely from the tube into the atmosphere it can be shown that

$$K_{\text{loss}} = K_{\text{out}} = 1 \Leftrightarrow \Delta P_{\text{loss}} = \frac{\rho_f V^2}{2}. \tag{7}$$

This remarkable result means that the kinetic energy of the conveyed flow is entirely and irreversibly lost by the outflowing jet and no pressure drop takes place at the exit section, implying that static pressure inside the tube is equal to the ambient pressure outside the tube. Hence, the boundary conditions which hold at the outlet section, if considered as a part of the tube flow, are as follows:

$$P_{\text{out}} = P_a \quad , \quad V_{\text{out}} = V. \tag{8}$$

According to conditions (8), the outflow from a pipe exit is shaped as a cylindrical jet at ambient pressure P_a and with the same velocity as in the discharging tube. In reality, downstream of the tube outlet, the jet is destroyed over a characteristic length $\mathcal{L}_c$ due to viscous friction. In contrast, if the outlet is considered as a part of the external fluid, which is at rest, the appropriate boundary conditions become:

$$P_{\text{out}} = P_a \quad , \quad V_{\text{out}} = 0, \tag{9}$$

meaning that the condition is applied in fact at the distance $\mathcal{L}_c$ from the tube outlet. In both cases, it is not needed to specify the actual value of $\mathcal{L}_c$ and the latter may be assumed arbitrarily small.

The streamlines corresponding to the inflow into a pipe entrance markedly differ from those which hold at a pipe exit. They are typically converging from all directions available outside the tube entrance, as sketched in Figure 1. Furthermore, flow conditions highly depend on the detailed geometry of the inlet and so does the inlet loss coefficient K_{in}, as also indicated in Fig. 1 for three contrasting cases, namely the thin wall tube with unbaffled inlet, tube flush with a wall at right angle and finally the gently rounded wall entrance. Depending on the cases, the loss coefficient changes by one to two orders of magnitude, see Blevins [16], Idel'cik [17]. To drive a given mean flow velocity V into the tube, the static pressure to be prescribed at the exit of the aspirating tube is found to be:

$$P_{\text{out}} = P_a - \frac{\rho_f V^2}{2}\left(K_{\text{in}} + 1 + \frac{fL}{D}\right). \tag{10}$$

The coefficient fL/D accounts for the pressure drop due to fluid friction at the wall of the pipe of length L and hydraulic diameter D (cf. Darcy-Weissbach law, see refs. [16] or [17]).

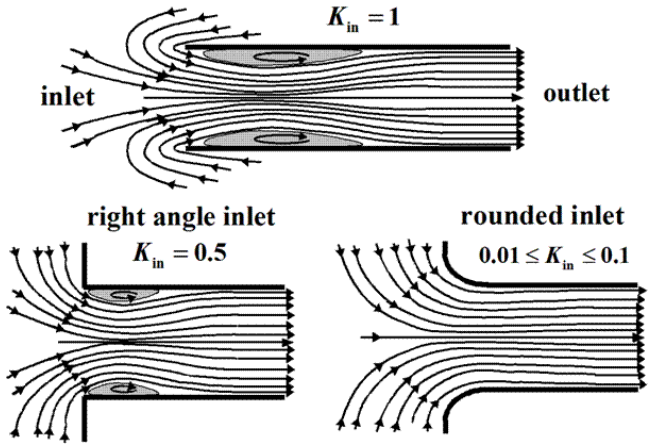

Figure 1. *Pressure drop at a tube inlet*

The conditions at the external side of the tube inlet deserve a special comment since they are less intuitive than in the outlet case. The conditions found to be consistent with the concept of pressure loss and with experimental data read

$$P_{\text{in}} = P_a \quad , \quad V_{\text{in}} = 0, \tag{11}$$

where the inlet is considered as a part of the external fluid at a distance $\mathcal{L}'_c$ of the tube inlet, which again may be assumed to be arbitrarily small, in analogy with the discharging outlet case. If the inlet is considered as a part of the internal fluid, the conditions (11) are replaced by the following ones:

$$P_{\text{in}} = P_a - \frac{1}{2}\rho_f V^2\left(K_{\text{in}}+1\right) \quad , \quad V_{\text{in}} = V. \tag{12}$$

Application of these basic concepts, whose validity is firmly established in the steady case of motionless tubes, to the deceptively 'simple' riddle asked by Richard Feynman as a physics student at Princeton circa 1940 about the rotating lawn sprinkler (see Feynmann [18] Forrester [19], Wheeler [20], Païdoussis [3]) leads to the answer that in aspirating flow the sprinkler is expected to remain at rest. The driving torque is determined using the control volume method. As sketched in Fig. 2, the control volume is defined as an arm of the sprinkler delimited by the cross-sections at the rotation axis of the device and at the discharging or aspirating pipe end. As a well known result, the net force exerted by the flowing fluid on the arm at rest $\left(\Omega = 0\,,\, \vec{u} = \vec{i}\right)$ is:

$$\vec{F}_{\mathcal{W}} = \left[\left(\bar{P} + \rho_f V^2\right) S_f \vec{\ell}\right]_{\text{out}}^{\text{in}}, \tag{13}$$

where $\bar{P} = P - P_a$ is the pressure counted above the external ambient pressure and V is the mean flow velocity, both quantities referring to the internal fluid, that is within the control volume.

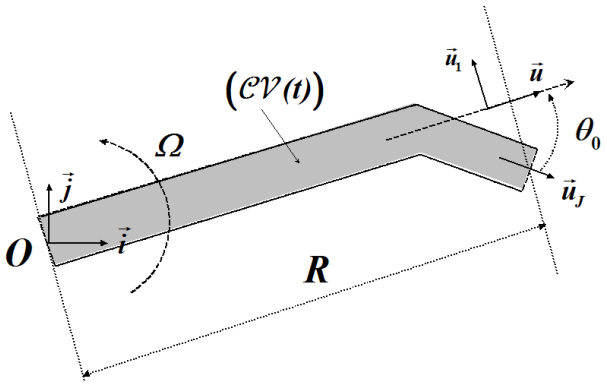

Figure 2. *Sprinkler arm considered as the control volume. Here $\vec{i}, \vec{j}$ designate the unit vectors of the non rotating frame of reference, while $\vec{u}, \vec{u}_1$ are those of the co-rotating frame*

The driving torque exerted on the arm at rest follows immediately as

$$\vec{\mathcal{M}}_{\mathcal{W}} = R\left(\vec{i} \times \vec{F}_{\mathcal{W}}\right) = RF_{\mathcal{W}j}\vec{k}. \tag{14}$$

Considering the discharging case, $\vec{\ell}_{\text{out}} = \cos\theta_0 \vec{i} - \sin\theta_0 \vec{j}$ and $\vec{\ell}_{\text{in}} = \vec{u} = \vec{i}$, whence

$$\vec{\mathcal{M}}_{\mathcal{W}} = -RS_f\left(\bar{P}_{\text{out}} + \rho_f V_{\text{out}}^2\right)\left(-\sin\theta_0\right)\vec{k} \Rightarrow$$
$$\vec{\mathcal{M}}_{\mathcal{W}} = RS_f \rho_f V^2 \sin\theta_0 \vec{k}. \tag{15}$$

The result is arrived at as a direct application of conditions (8). It may also be noted that it would be the same in a frictionless plug flow: $\bar{P}_0 = 0; V_0 = V$. In the aspirating case, $\vec{\ell}_{\text{out}} = -\vec{i}$ and $\vec{\ell}_{\text{in}} = -\cos\theta_0 \vec{i} + \sin\theta_0 \vec{j}$, whence

$$\vec{\mathcal{M}}_{\mathcal{W}} = RS_f\left(\bar{P}_{\text{in}} + \rho_f V_{\text{in}}^2\right)\sin\theta_0 \vec{k} \Rightarrow$$
$$\vec{\mathcal{M}}_{\mathcal{W}} = \frac{1}{2}\rho_f V^2\left(1 - K_{\text{in}}\right) RS_f \sin\theta_0 \vec{k}. \tag{16}$$

Substituting the appropriate value $K_{\text{in}} = 1$ for the pressure loss coefficient into (16) the torque is thus found to be nil, a value which clearly differs from that which would be obtained using the frictionless plug flow model, where no distinction can be made between the discharging and the aspirating cases. Moreover, it can also be argued that even if the geometry of the tube intake is modified with respect to the unbaffled case, the above result remains valid, since the change in the flow induced force at the tube wall is expected to be exactly balanced by the force exerted at the tube intake. As a typical example amenable to short calculation, we may consider an intake device shaped as an abrupt change in cross sectional area, see Fig. 3. Denoting by P_2 the pressure and V_2 the velocity at the elbow, the force exerted on the elbow in the $\vec{\ell}_1$ direction is

$$\vec{F}_{\text{elbow}}.\vec{\ell}_1 = \left(\rho_f V_2^2 + P_2 - P_a\right)S_2 = \left(\rho_f V_2^2 + \bar{P}_2\right)S_2, \tag{17}$$

while the force exerted on the intake component reads as

$$\vec{F}_{\text{compo}}.\vec{\ell}_1 = \left(\rho_f V_1^2 + P_1\right)S_1 - \left(\rho_f V_2^2 + P_2\right)S_2 - P_a\left(S_1 - S_2\right),$$
$$\vec{F}_{\text{compo}}.\vec{\ell}_1 = \left(\rho_f V_1^2 \bar{P}_1\right)S_1 - \left(\rho_f V_2^2 + \bar{P}_2\right)S_2. \tag{18}$$

Hence, the net force exerted on the whole pipe reads

$$\left(\vec{F}_{\text{elbow}} + \vec{F}_{\text{compo}}\right).\vec{\ell}_1 = \left(\rho_f V_1^2 + \bar{P}_1\right)S_1. \tag{19}$$

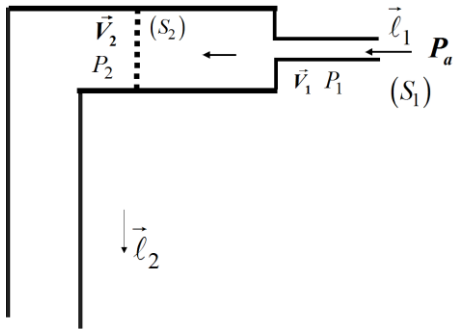

Figure 3. *Elbow terminated by an abrupt change of section*

The intermediate result (19) clearly indicates that the net force does not depend on the actual value of the pressure loss coefficient of the intake component set at the inlet of the elbow. This is precisely because the force exerted on the component cancels out exactly that at the inlet of the elbow. Furthermore, the net force is precisely zero, since $\bar{P}_1 = -\rho_f V_1^2$ in agreement with condition (12), where again $K_{\text{in}} = 1$.

Actually, theoretical justification of such behavior and even validity of it based on experiment gave rise to a rather abundant

and controversial literature, see in particular Weyland & Patterson, [21], Forrester [19], Hsu [2] Berg et al. [22], Collier [23], Païdoussis, [3,7], Païdoussis & Tétreault-Friend, [24]. This motivated us to repeat the experiment. The device devised and built by J. Antunes is shown in Figure 4. Possibility was provided to set nozzles of different geometries with the objective to check whether the behavior of the inverse sprinkler depends, or not, on the pressure drop at the aspirating intake. To avoid the risk of flooding the lab, due to excessive pressurization in an attempt to make the aspirating device rotate, experiments were carried out using air instead of water. As in the similar experiment conducted by Païdoussis & Tétreault-Friend [24], great care has been provided to minimize friction at the bearing supporting the sprinkler arms. In our experiment in the aspirating case, the sprinkler was invariably found to remain at rest, in contrast with the McGill experiment where rotation or oscillations of the sprinkler were initiated above a minimum air-flow. The likely reason for having missed such exciting behavior is the limited range of flow velocity available in our experimental set-up, where a domestic air cleaner was used to drive the flow. Even if validity of flow conditions (11), or (12) equivalently, is limited to a range of low flow velocities, it is nevertheless of interest to investigate their effect on the dynamics of a vibrating pipe.

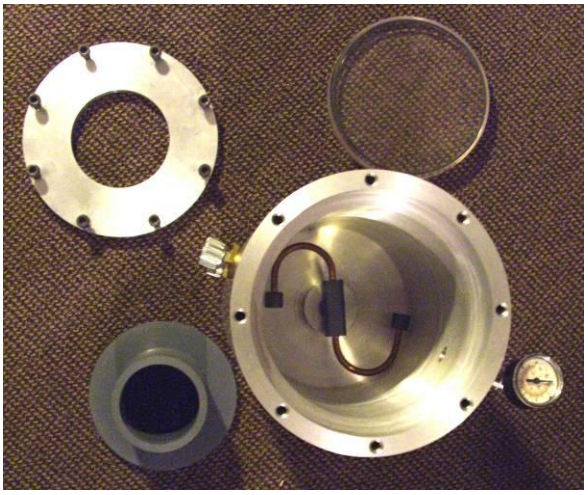

Figure 4. *Sprinkler experimental model*

As suggested first by Pramila [25] and further elaborated in Païdoussis [4,5] and Kuiper & Metrikine [8], a second type of flow-condition to be considered is the change of flow momentum at the tube intake and the related unsteady force exerted on it. Within the vibrating pipe, the velocity is the same either in the aspirating mode or in the discharging mode:

$$\vec{V}_L = V\vec{i} + \left(\frac{\partial Z_L}{\partial t} + V \frac{\partial Z_L}{\partial x} \right) \vec{k}. \tag{20}$$

where V is taken positive for discharging flow and negative for aspirating flow and $Z_L = Z(L,t)$.

In contrast to the discharging case, the mean velocity of the aspirated flow outside the tube, denoted $\vec{V}_{\text{out}}$, is likely to differ from $\vec{V}_L$. The net force $\vec{F}_L$ related to the momentum change reads

$$\vec{F}_L = -\frac{d\left(\vec{P}_{\text{in}} - \vec{P}_{\text{out}}\right)}{dt}, \tag{21}$$

where $\vec{P}_{\text{in}}$ means the fluid momentum within the tube and $\vec{P}_{\text{out}}$ that outside the tube. The minus sign means that we consider here the force exerted by the flowing fluid on the tube. These quantities are calculated referring to the amount of fluid conveyed during a small interval of time $t - t_0$, a procedure devised in Benjamin [26] to derive the Lagrange equations of the coupled system in a natural and elegant way. So the inlet values of the fluid momentum inside and outside of the tube, respectively, are expressed as

$$\begin{aligned} \vec{P}_{\text{in}} &= m_f |V|(t - t_0)\left(V\vec{i} + \left(\frac{\partial Z}{\partial t} + V \frac{\partial Z}{\partial x} \right) \vec{k} \right), \\ \vec{P}_{\text{out}} &= m_f |V|(t - t_0)\vec{V}_{\text{out}}. \end{aligned} \tag{22}$$

Since the time interval can be made arbitrarily small, the time differentiation in (22) is followed by the limiting process $t \to t_0$ to get rid of the secular term. Accordingly, the inlet force follows as

$$\vec{F}_L = -m_f |V| \left(V\vec{i} + \left(\frac{\partial Z_L}{\partial t} + V \frac{\partial Z_L}{\partial x} \right) \vec{k} - \vec{V}_{\text{out}} \right). \tag{23}$$

Of course, the actual value of $\vec{F}_L$ depends critically on that of $\vec{V}_{\text{out}}$. To the author's knowledge at least, there is no theoretical solution to the problem, while to be reliable CFD solutions ought to be checked by comparison with other methods. Therefore, an experimental approach is clearly needed where the aim is to infer $\vec{F}_L$ from the dynamical response of the pipe. Experimental procedures and results obtained so far make the object of a companion paper by Debut et al. [1]. Here, the dynamical response of two elementary pipe systems, as predicted by linear theory, is discussed in relation with a few more or less plausible assumptions concerning the unknown field $\vec{V}_{\text{out}}$. As a first working hypothesis, $\vec{V}_{\text{out}}$ is written as

$$\vec{V}_{\text{out}} = V\left(\alpha\vec{i} + \beta \frac{\partial Z}{\partial x}\vec{k} \right) + \gamma \frac{\partial Z}{\partial t}\vec{k}, \tag{24}$$

where α, β, γ are treated as free parameters to be determined. The assumptions concerning $\vec{V}_{\text{out}}$ contemplated in Païdoussis et al. [4] or Kuiper & Metrikine [8] follow as particular cases. For instance, the choice $\alpha = \beta = \gamma = 1$ corresponds to the less plausible case of a fully matched aspirating flow $\vec{V}_{\text{out}} = \vec{V}_{\text{in}}$

where $\vec{F}_L$ vanishes to zero. As suggested in Païdoussis et al. [4] the set $\alpha=\beta=1, \gamma=0$ may stand for a more plausible assumption of partial flow adaptation, where $\vec{V}_{\text{out}}$ is parallel to the deflected pipe axis, while it does not adapt to the lateral translation of the tube, in such a manner that the inlet force becomes

$$\vec{F}_L = -m_f |V| \frac{\partial Z_L}{\partial t}\vec{k}. \tag{25}$$

Finally, if the outside flow fully ignores the fluctuations related to the motion of the pipe intake while $\alpha=1$, the inlet force reads:

$$\vec{F}_L = -m_f |V| \left(\frac{\partial Z_L}{\partial t} + V \frac{\partial Z_L}{\partial x} \right)\vec{k}. \tag{26}$$

More generally, the force predicted by this kind of model is of the type

$$\vec{F}_L = -m_f |V| \left\{ \begin{array}{c} V(1-\alpha)\vec{i} \\ \left(V(1-\beta)\dfrac{\partial Z_L}{\partial x} + (1-\gamma)\dfrac{\partial Z_L}{\partial t} \right)\vec{k} \end{array} \right\}. \tag{27}$$

Consequences of these variants of the same basic aspirating flow model are investigated in the next section considering two mechanical systems especially selected for their simplicity and feasibility as experimental devices. Being aware of the difficulties in performing reliable and easy to interpret experiments using flexible and submerged aspirating tubes, the choice was made to go back to the articulated rigid pipe elements investigated first in Benjamin [26,27]. Pertinence of such a choice lies in the fact that the present work is entirely focused on the flow conditions at the pipe entrance (or outlet in the case of discharging flow) which can be reasonably assumed to hold independently of the tube flexibility. Furthermore, articulated chains of rigid pipes are also selected for their conceptual and experimental convenience in providing discretized models of flexible pipes of the lumped type which have the advantage of being physically feasible in contrast with those stemming from modal expansion or finite element models.

3 DYNAMICS OF ARTICULATED PIPE SYSTEMS

3.1 Single pipe element supported by a rotational spring

The simplest possible system to deal with is shown in Fig. 5. It consists of a straight and uniform tube element of length L conveying an incompressible fluid. In the discharging case, tube entrance is supported by an elastic articulation and the other end is free. We are interested in the dynamics of the system when restricted to motions of small amplitude taking place in the plane of the figure. The latter is assumed to be horizontal or vertical, according to gravity being discarded or not. This 1-DOF system is described by using the angular variable θ. Derivation of the equation of motion in flowing fluid is straightforward. The flow-structure coupling force (3) reduces to the Coriolis component and the modal equation in the vertical layout reads

$$\left\{ \left(K_\theta + \frac{gM_eL}{2} \right) + i\omega\left(C_\theta + M_a V_0 L \right) - \omega^2 \frac{M_e L^2}{3} \right\}\theta = L\vec{i} \times \vec{F}_L. \tag{28}$$

K_θ is the rotational stiffness coefficient of the articulation and g is the acceleration of gravity. Dissipation due to friction at the articulation is modelled as an equivalent viscous torque of damping coefficient C_θ. M_s designates the mass of the tube and M_a is the fluid added mass for a lateral motion, equal here to the physical mass M_f of the fluid contained in the pipe element. Finally, $M_e = M_s + M_f$ is the equivalent mass of the pipe filled with fluid.

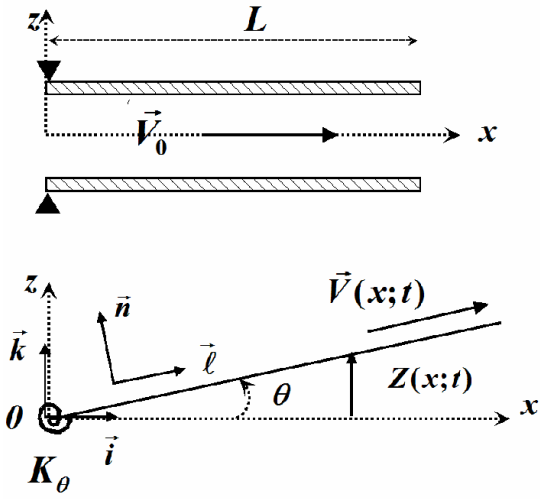

Figure 5. *Rigid tube provided with an elastic articulation at one end*

Equation (28) is suitably recast in dimensionless form as

$$(1+\Gamma) + 2i\Omega\left(\sqrt{(1+\Gamma)}\varsigma_0 + \frac{3\sqrt{\mu_a}V_R}{2} \right) - \Omega^2 = \bar{\mathcal{M}}_L, \tag{29}$$

where the reduced quantities are defined as follows:

$$\Omega = \frac{\omega}{\omega_0} = \omega\sqrt{\frac{M_eL^2}{3K_\theta}}, \quad \Gamma = \frac{M_e g L}{2K_\theta}, \quad \mu_a = \frac{M_a}{M_s + M_a},$$
$$V_R = \frac{V\sqrt{\mu_a}}{\omega_0 L}, \quad \bar{\mathcal{M}}_L = \frac{3K_\theta L \vec{F}_L.\vec{k}}{M_e L^2}. \tag{30}$$

In discharging flow $\vec{F}_L \equiv 0$ while the Coriolis term is dissipative in nature. Hence, the reduced damping $\varsigma(V_R)$ is expected to increase linearly with the reduced flow velocity V_R, while the natural frequency is expected to decrease according to the parabolic law $f \propto \sqrt{1-\varsigma^2(V_R)}$, vanishing to zero when damping becomes critical $\varsigma(V_{RD}) = 1$. In the range $V_R \geq V_{RD}$

the oscillator is overdamped. In aspirating flow, both the stiffness and the damping operators of the oscillator equation may become dependent on V_R which is negative:

$$\bar{K}(V_R) = 1 + \Gamma - (1-\beta)V_R^2,$$
$$\bar{C}(V_R) = 2\sqrt{1+\Gamma}\,\varsigma_0 - 3\sqrt{\mu_a}\,|V_R|\,\gamma. \tag{31}$$

Accordingly, response of the oscillator is expected to be insensitive to the aspirating flow, if and only if $\beta = 1$ and $\gamma = 0$. Otherwise, divergence or flutter may be expected to occur, depending on the values of the oscillator parameters in still fluid and those of the aspirating flow. Furthermore, even if the experiment is not conducted up to the critical flow velocity for instability to occur it may be reasonably expected that the changes in the oscillator stiffness and damping coefficients are amenable to quantitative measurement as $|V_R|$ is increased, while validity of the procedure can be conveniently checked by performing tests in discharging flow.

3.2 Articulated pair of rigid pipe elements

Once the values of the aspirating flow parameters β and γ have been elucidated, the depressurization conditions (11) or (12) may be investigated by considering articulated chains of rigid pipe elements where curvature of a fully flexible pipe is discretized as abrupt changes in flow direction at the junction between two adjacent tube elements. This enables us to account for the flow-induced centrifugal and pressurization forces which are missing in the 1-DOF system considered just above. The system considered here is the hanging pair of tubes sketched in Fig. 6.

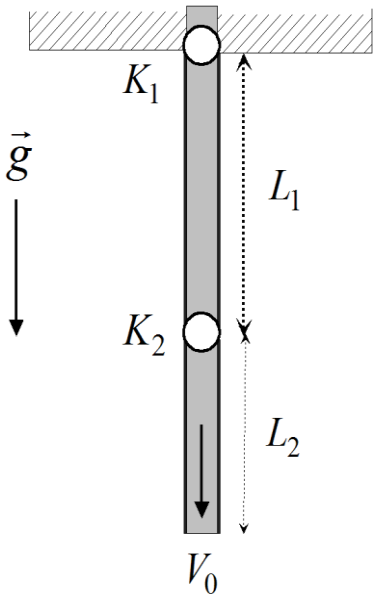

Figure 6. *Pendular system of two articulated rigid tubes vibrating about the stable static equilibrium*

The system set free at the bottom end is governed by the modal equation, written in matrix form as:

$$\left\lfloor \left\lfloor K(V) \right\rfloor + i\omega \left\lfloor C(V) \right\rfloor - \omega^2 \left[M_e \right] \right\rfloor [q] = [Q_L],$$
$$\left[K(V) \right] = \left[K_e \right] + \left[K_g \right] + \left(m_a V^2 + P_p \right) \left[K_V \right],$$
$$\left[C(V) \right] = \left[C_s \right] + m_a V \left[C_V \right], \tag{32}$$
$$\left[M_e \right] = \left[M_s \right] + \left[M_a \right].$$

In eq. (32) the generalized displacement vector is defined as $[q]^T = [\theta_1 \quad \theta_2]$, where θ_1 and θ_2 are the small angles of the tube elements to the vertical. $\left[K_e \right]$ means the stiffness matrix which accounts for the elasticity of the articulations, while $\left\lfloor K_g \right\rfloor$ is the prestress matrix related to gravity. $\left[M_s \right]$ means the mass matrix of the solid part of the system, while $\left[M_a \right]$ is the added mass matrix related to the internal fluid. All these matrices are symmetrical positive definite as suitable for conservative operators. They are written as:

$$\left[K_e \right] = K_2 \begin{bmatrix} 1+\kappa & -1 \\ -1 & 1 \end{bmatrix},$$
$$\left[K_g \right] = \frac{M_e g L_1}{2} \begin{bmatrix} 1+2\Lambda & 0 \\ 0 & \Lambda^2 \end{bmatrix},$$
$$\left[M_s \right] + \left[M_a \right] = \left(\frac{M_e L_1^2}{3} \right) \begin{bmatrix} (1+3\Lambda) & 1.5\Lambda^2 \\ 1.5\Lambda^2 & \Lambda^3 \end{bmatrix}, \tag{33}$$
$$M_e = M_s + M_f = \left(m_s + m_f \right) L_1,$$

with the following reduced quantities:

$$\Lambda = \frac{L_2}{L_1};\ \kappa = \frac{K_1}{K_2};\ \omega_0 = \sqrt{\frac{3K_2}{m_e L_1^3}};\ \Omega = \frac{\omega}{\omega_0}. \tag{34}$$

The centrifugal matrix $\left\lfloor K_V \right\rfloor$ and the Coriolis matrix $\left\lfloor C_V \right\rfloor$ are

$$m_f V^2 \left[K_V \right] = m_f V^2 L_1 \begin{bmatrix} -1 & 1 \\ 0 & 0 \end{bmatrix}$$
$$m_f V \left[C_V \right] = m_f V L_1^2 \begin{bmatrix} 1 & 2\Lambda \\ 0 & \Lambda^2 \end{bmatrix} \tag{35}$$

Both of them are nonsymmetrical indicating that they govern nonconservative effects, as must be expected.

Finally, small dissipation taking place at the articulations can be described by a viscous damping matrix of the type

$$\left[C_s \right] = C_2 \begin{bmatrix} 1+c & -1 \\ -1 & 1 \end{bmatrix} \tag{36}$$

where $c = C_1 / C_2$ is the ratio of the damping coefficient associated with the first articulation over that associated with the second articulation. However, to conduct tests in aspirating flow it is necessary to submerge the lower tube element, partly at least, in the water of the feeding tank from which fluid is

sucked. Dissipation due to friction in the external fluid is likely to be non-negligible. It may be accounted for by a viscous damping matrix of the type:

$$\left[C_f\right] = C_f \begin{bmatrix} \Lambda - \eta & \dfrac{\Lambda^2 - \eta^2}{2} \\ \dfrac{\Lambda^2 - \eta^2}{2} & \dfrac{\Lambda^3 - \eta^3}{3} \end{bmatrix} \tag{37}$$

The ratio $\eta = H / L_1$ means the non submerged length of the lower tube over the length of the first tube. It is a fact of common experience that neither solid damping nor fluid induced damping is amenable to modeling. Therefore the current practice is to adjust heuristically the coefficients C_1, C_2 and C_f to the proper values using experimental data in air and in still water.

Substantial dissipation could also be expected at the free level due to excitation of water waves, a priori at least. As detailed in Axisa & Antunes [29], analytical formulation of damping induced by radiation of water waves is not an easy task. However, in the case the free surface is bounded by the wall of the water tank, radiated energy is in fact reflected back to the vibrating structure, a substantial part of it at least. Moreover, as indicated in the companion paper, water waves can be efficiently prevented to occur in the experimental device by providing the free level with a rigid plate. Then, for all of these reasons, no attempt was made in the present study to include radiation damping into the theoretical analysis.

In discharging flow the generalized force vector $\left[Q_L\right]$ is nil. Solving the complex modal equation (32) is nowadays standard routine using commercially available software. Here we use MATLAB. Matrix equation (32) is first recast in dimensionless form as

$$\left|\left[\kappa(u)\right] + i\Omega u\sqrt{\mu_a}\left[c_u\right] - \Omega^2\left[\mu\right]\right|\left[\theta\right] = \left[0\right],$$

$$\left[\kappa(u)\right] = \left[\kappa_e\right] + \Gamma\left[\kappa_g\right] + \frac{u^2\left(2+\pi_p\right)}{2}\left[\kappa_u\right], \tag{38}$$

$$\mu_a = \frac{m_a}{m_e}; \quad u = \frac{V\sqrt{\mu_a}}{\omega_0 L_1}; \quad \pi_p = \frac{2P_p}{\rho_f V_0^2}.$$

The most salient features of the dynamical behavior predicted by linear theory are summarized in the stability plots of Fig.7, which refer to the idealized case where damping in still fluid is discarded. Provided gravity is sufficiently high, stability is lost either via flutter of the so-called "phase-opposition mode" $(\theta_1\theta_2 < 0)$ or by divergence of the so-called "in-phase mode" $(\theta_1\theta_2 > 0)$, depending on whether μ_a is smaller or larger than a transition value which is a decreasing function of Γ. On the stability lines, transition from flutter to divergence is marked by a singular point with a finite tangential discontinuity. The tangent is horizontal at the line portion related to divergence while it is tilted at the line portion related to flutter. Moreover, if Γ is sufficiently large, the slope of the tilted tangent is negative. Accordingly, if flow velocity is progressively increased in that part of the stability line, the system is found to lose stability via flutter, then to be restabilized in a narrow range of flow velocity at least and destabilized eventually via divergence.

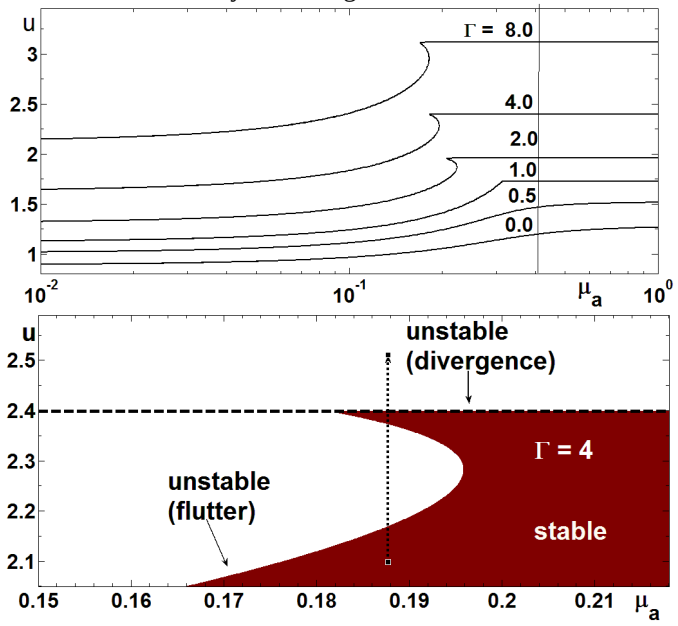

Figure 7. *Stability maps for the articulated pair of rigid tube elements versus the added-mass ratio (dashed line: flutter, full line: divergence)* $\Lambda = 1, \pi_p = 0$

Turning now to the case of aspirating flow, $\left[Q_L\right]$ is derived using the virtual work of the end force:

$$\delta\mathcal{W}_L = \left[\delta q\right]^T\left[Q_L\right] = \delta\vec{Z}_L.\vec{F}_L. \tag{39}$$

The virtual displacement is found to be:

$$\delta\vec{Z}_L = \left(L_1\delta\theta_1 + L_2\delta\theta_2\right)\vec{k} - \left(L_1\theta_1\delta\theta_1 + L_2\theta_2\delta\theta_2\right)\vec{i}, \tag{40}$$

where the axial component stems from the axial displacement (5). Substituting (40) and (27) into (39) and collecting the coefficients of the generalized displacements $\delta\theta_1$, $\delta\theta_2$ gives $\left[Q_L\right]$ as the sum of a centrifugal component and a Coriolis component:

$$\begin{aligned} & m_f\left|V\right|VL_1\begin{bmatrix} 1-\alpha & \beta-1 \\ 0 & \Lambda(\beta-\alpha) \end{bmatrix}\begin{bmatrix} \theta_1 \\ \theta_2 \end{bmatrix}, \\ & i\omega m_f\left|V\right|(1-\gamma)L_1^2\begin{bmatrix} 1 & \Lambda \\ \Lambda & \Lambda^2 \end{bmatrix}\begin{bmatrix} \theta_1 \\ \theta_2 \end{bmatrix}. \end{aligned} \tag{41}$$

The net flow-structure coupling force acting on the system in aspirating flow follows by substituting (41) into the left hand-side of the modal equation (38). Of course, it also comprises centrifugal and Coriolis operators expressed in dimensionless form as

$$u^2\left\{\left(\frac{2+\pi_p}{2}\right)\begin{bmatrix}-1 & 1\\ 0 & 0\end{bmatrix}+\begin{bmatrix}1-\alpha & \beta-1\\ 0 & \Lambda(\beta-\alpha)\end{bmatrix}\right\}, \quad i\varpi|u|\begin{bmatrix}-\gamma & -(1+\gamma)\Lambda\\ (1-\gamma)\Lambda & -\gamma\Lambda^2\end{bmatrix}. \tag{42}$$

A priori, the relevant value of the pressurization coefficient is $\pi_p = -2$, in such a manner that the first term in the centrifugal component is nil, in full agreement with the observation that the sprinkler remains at rest in aspirating flow, provided flow velocity is sufficiently low, at least, cf. Païdoussis & Tétreault-Friend [24]. Nevertheless, departure from this steady value is also plausible as resulting from a possible unsteady component of the pressure drop related to the tube motion, or/and resulting from the follower axial force induced by suction of the external fluid at the aspirating entrance, as suggested in Païdoussis et al. [4]. The second term of the centrifugal matrix and the Coriolis matrix depend on the outside flow direction at the intake. As a particularly interesting case, the partially matched flow $\alpha = \beta = 1, \gamma = 0$ is found to be gyroscopically conservative since the flow-structure coupling operator reduces to a skew-symmetrical Coriolis matrix. If the outside flow fully ignores the fluctuations related to the motion of the pipe inlet $(\alpha = 1, \beta = \gamma = 0)$ the system is prone to flutter instability as the Coriolis matrix leads again to gyroscopic coupling while the centrifugal component acts as a follower force.

Tube dynamics is further described below using a typical example selected for its feasibility as an experimental set-up. Two identical steel tube elements of length $L = 40$ cm, external radius $R_e = 1$ cm, thickness $h = 2$ mm, are articulated using an anisotropic spring system to restrict motion within a single vertical plane. The related spring coefficient is so soft that the gravity parameter is fairly high, $\Gamma = 1$. The conveyed fluid is water, implying an added mass ratio $\mu_a \simeq 0.19$. The lower tube element is assumed to be fully submerged into the feeding tank ($\eta = 0$). The mode shapes and related natural frequencies in still fluid are shown in Fig. 8.

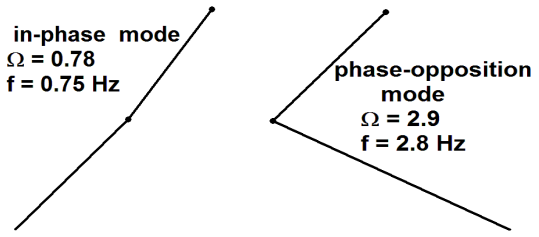

Figure 8. *Real mode shapes and natural frequencies in still fluid:* $\mu_a = 0.19, \Gamma = 1, \Lambda = 1, \pi_p = 0, \eta = 0$

Reduced damping induced by solid friction at the articulations is found to be much less in the in-phase mode than in the phase-opposition mode, while the opposite occurs as the damping induced by external fluid friction is concerned. For the present purpose, the value of the reduced damping in still fluid may be set to a unique value of a few percent in both modes. The computations presented here were carried out by assuming the damping matrix $[C] = 0.02\left([C_s] + 5[C_f]\right)$, which leads to $\varsigma(u = 0) \simeq 2\%$. Fig. 9 refers to the discharging flow case. It displays the real frequency $R(\Omega)$ and the damping ς plots of the system versus the mean flow velocity in dimensionless form, using the scaling factors defined in eqs. (34), (38).

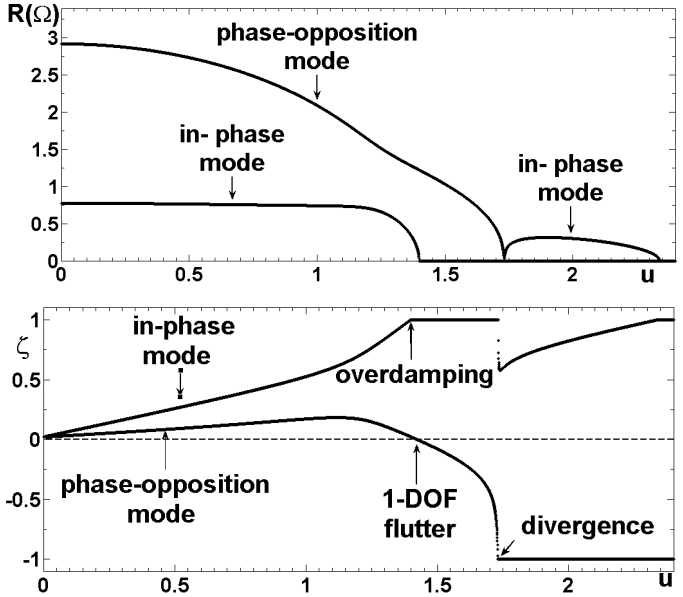

Figure 9. *Frequency and damping plots vs flow velocity in discharging flow:* $\mu_a = 0.19, \Gamma = 1, \Lambda = 1, \pi_p = 0, \eta = 0$

Frequency of the in-phase mode vanishes to zero at about $u \simeq 1.42$, where overdamping occurs up to $u \simeq 1.75$. Then, in the interval $1.75 < u < 2.3$, damping assumes large, though undercritical, values and finally in the range $u > 2.3$, the in-phase mode is overdamped again. Turning to the phase-opposition mode, frequency is also decreasing as mean flow velocity increases. Threshold for divergence occurs at $u_{Cd} \simeq 1.75$, that is essentially the same flow velocity at which the in-phase mode leaves the first overdamped domain. More important, damping is increasing first to a maximum value of about 18% at $u \simeq 1.15$ and then is found to decrease down to the divergence critical value of -1. Flutter is expected to occur above the threshold value $u_{Cf} \simeq 1.42$, which corresponds also to the threshold velocity at which the in-phase mode becomes overdamped for the first time. In physical units, flutter instability is expected in the phase-opposition mode at $V_{Cf} \simeq 8$m/s. To lose stability via divergence the springs ought

to be four times softer than the value assumed here, in such a manner that Γ would be equal to 2 instead of 1, see Fig 7.

Fig. 10 to 13 refer to aspirating flow cases, as indicated by the negative values of u in the frequency and damping plots, where distinct assumptions are made concerning the external flow velocity $\vec{V}_{\text{out}}$. Partially adapted flow model is considered first where mean flow velocity is the same just inside and outside the tube intake except the lateral component ($\gamma = 0$). As $|V|$ is increased due to flow-induced gyroscopic coupling, the natural frequency of the phase-opposition mode is found to increase, while that of the in-phase mode is found to decrease. Damping of both modes is found to decrease with $|V|$. Nevertheless, no linear instability of any kind is expected to occur even if $|V|$ is assumed to tend to infinity.

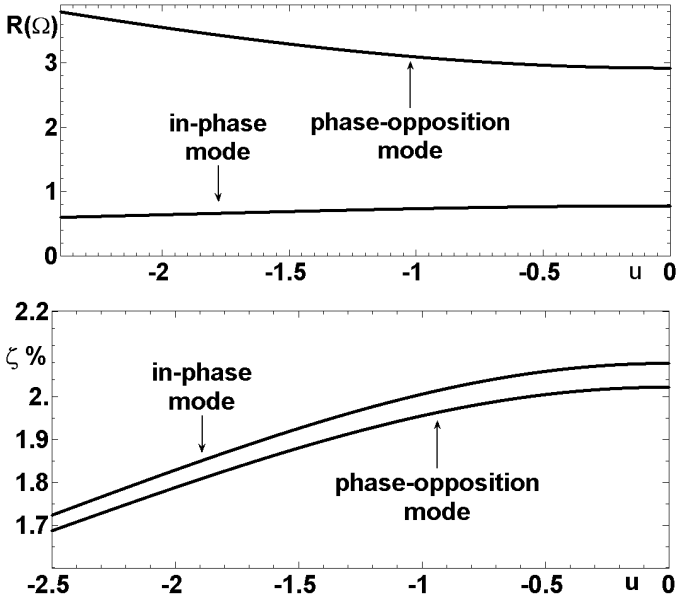

Figure 10. *Frequency and damping plots in aspirating flow: Partially adapted flow model* $\alpha = \beta = 1, \gamma = 0$

Fig. 11 refers to the case where some mismatch is also assumed to occur in the axial flow component. Restricting discussion to the limited range of flow-velocity less than $|u| = 2.5$, that is about 14 m/s, the most conspicuous difference with respect to the former case resides in the fact that frequency of both modes increases with $|V|$, as a consequence of the tensioning effect of the flow-induced centrifugal matrix (42) which reduces here to an axial tensioning matrix, conservative and positive definite. Another point worth to be noted is that damping of the in-phase mode decreases faster with $|u|$ than that of the phase-opposition mode. Nevertheless damping of both modes is found to remain positive at any $|u|$ and no instability may be induced by changing the value of the intake flow parameter α, that is the vertical component of the flow velocity.

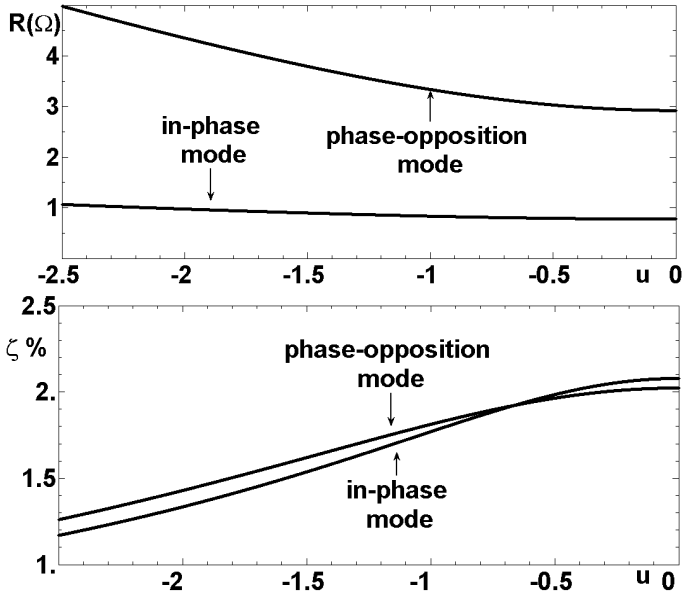

Figure 11. *Frequency and damping plots in aspirating flow: Partially adapted flow model* $\alpha = 0.8, \beta = 1, \gamma = 0$

In the case depicted in Fig. 12 the outside flow is allowed to have a component in phase with the velocity of the vibrating intake. Even if the magnitude of this component is small, $\gamma = 0.025$ in the present example, drastic changes in the tube dynamics are expected to occur since the Coriolis matrix (42) becomes non conservative in nature. Actually, dynamic instability via flutter of the in-phase mode is expected beyond $u_{Cf} = 1.9$, that is about 10 m/s, a value not very far from that predicted in discharging flow. Of course by increasing the value of γ this threshold may be decreased down to very small values, while no instability occurs if γ assumes negative values.

Similarly, in Fig. 13 a mismatch is assumed in the unsteady tangential flow component $(\beta = 0.9)$. As a consequence, the centrifugal operator (42) describes a follower force. As could be expected, this also leads to drastic changes since the system is predicted to lose stability via flutter of the phase-opposition mode at $u_{Cf} \simeq -1.83$ while damping of the in-phase mode is rapidly increasing up to supercritical values. It is worth noticing that if β is assumed larger than unity, flutter is expected in the phase opposition mode while damping of the in-phase mode increases slightly with flow velocity.

Finally, it is worth noticing that any departure of the pressurization parameter π_p from the steady value $\pi_p = -2$ also gives rise to a net follower force in aspirating flow. As already mentioned above, physical origin of such a follower force could be the suction of fluid at the free-end cross-section of the lower tube element and possibly also the presence of an

unsteady component of the pressure drop. The destabilizing effect of these mechanisms is found to be qualitatively equivalent to that arising from the departure of β from the perfect matching value $\beta = 1$. Hopefully, distinction between the two cases may be possible since dynamics of the 1-DOF system is sensitive to β but not to π_p.

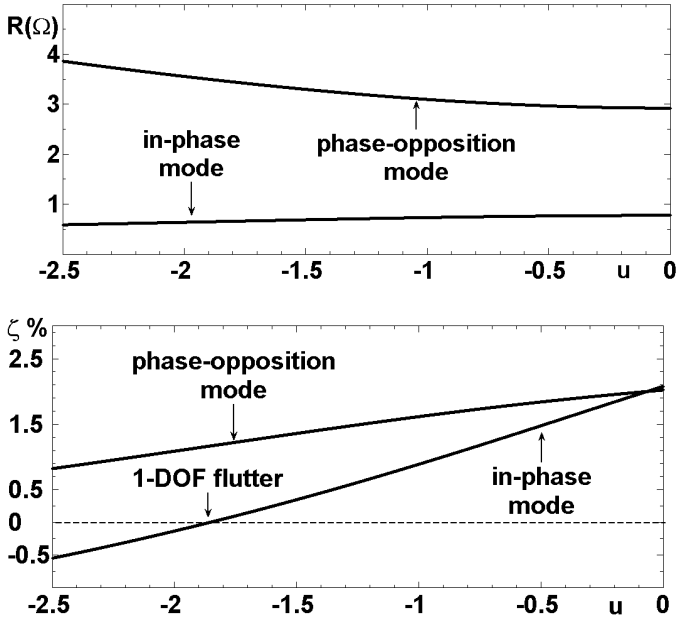

Figure 12. *Frequency and damping plots in aspirating flow: Partially adapted flow model* $\alpha = \beta = 1$, $\gamma = 0.025$

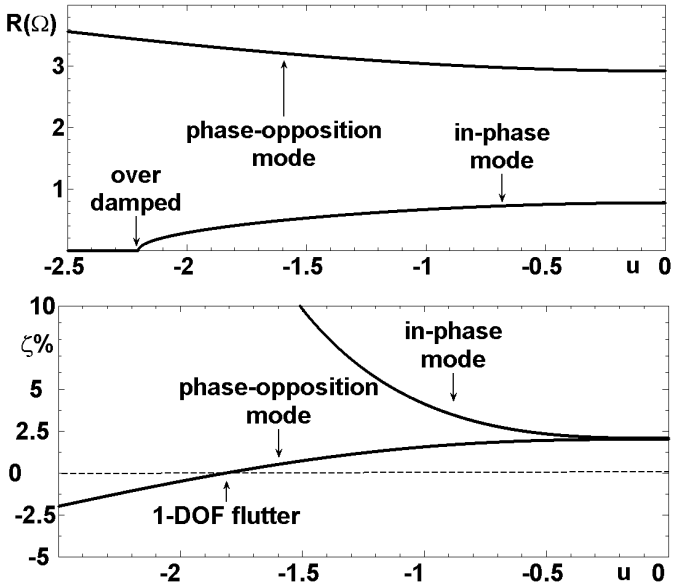

Figure 13. *Frequency and damping plots in aspirating flow: Partially adapted flow model* $\alpha = \beta = 0.9; \gamma = 0.$

4 CONCLUSION

In this paper, the flow conditions at an aspirating pipe inlet have been investigated in close relation to their imprint on the dynamics of the vibrating pipe; discussion being restricted to the linear models already considered in Païdoussis et al. (2005) which can be expected to hold at sufficiently low aspirating flow velocity, at least. The few distinct variants of the same basic model analyzed here are concerned with the mismatch between the mean flow properties just outside and just inside the tube intake. For that purpose it was found convenient to deal with discrete systems of articulated rigid pipes made as simple as possible (1-DOF and 2-DOF oscillators) instead of fully flexible pipes. As a major result, we arrive at the conclusion that even relatively small changes in the flow conditions assumed at the aspirating tube inlet are likely to lead to significant changes in the tube response. They can be used for experimental diagnoses, as further demonstrated in the companion paper by Debut et al. [1]. It will be shown that the experimental data produced so far at ITN are in fair agreement with the specific variant of the entrance flow model where depressurization is found to cancel completely the centrifugal force present in discharging flow, whatever the value of the pressure drop at the intake may be, while the lateral force cancels the Coriolis force induced by the conveyed flow. This model implies partial matching of the outside flow which is assumed to follow the axial direction of the deflected tube end. However the data do not preclude possibility for small correction terms, acting on the system damping, such as additional unsteady pressure loss or suction as suggested by Païdoussis et al. [4].

ACKNOWLEDGEMENTS

Thanks are due to the reviewers for their useful comments, as well as for the careful revision of the English text, which helped to improve significantly the content and the form of the paper.

REFERENCES

[1] Debut, V. Antunes, J. Axisa, F. , 2010, "Flow Conditions at the inlet of aspirating pipes. Part 2: Experiments," 7th International Symposium on Fluid-Structure Interaction, Flow-Sound Interaction, Flow-Induced Vibration and Noise. August 1-4th, 2010, Montreal, Canada.

[2] Hsu, L., 1988, "Inverse sprinklers: Two simple experiments and the resolution of the Feynmann-Forrester conflict," Am. J; of Physics 56, (4) pp. 307-308

[3] Païdoussis, M.P., 1998 Fluid-Structure Interactions Slender Structures and Axial Flow. Academic Press San Diego Chap. 4.

[4] Païdoussis, M.P., Semler, C., Wadham-Gagnon, M. , 2005, "A reappraisal of why aspirating pipes do not flutter at infinitesimal flow," J. Fluid and Structures 20 pp. 147-156

[5] Païdoussis, M.P., 2005, "Some unresolved issues in fluid-structure interactions," J. Fluid and Structures 20, pp. 871-890

[6] Païdoussis, M.P., 2008, "Dynamics of cantilevers subjected to internal and/or external axial flow: new developments and insights," 9th International Conference on Flow Induced Vibrations (FIV-2008), Zolotarev & Horacek eds, 30 June-3 July 2008, Prague, Czech Republic.
[7] Païdoussis, M.P., 2008, "The canonical problem of the fluid-conveying pipe and radiation of the knowledge gained to other dynamics problems across applied mechanics," J. of Sound and Vibration 310 pp. 462-492
[8] Kuiper G.L., and Metrikine A.V., 2005, "Dynamic stability of a submerged, free-hanging riser conveying fluid," J. of Sound and Vibration 280 pp. 1051-1065
[9] Kuiper G.L., Metrikine A.V., and Battjes, J.A., 2007, "A new time-domain drag description and its influence on the dynamic behavior of a cantilever pipe conveying fluid," J. of Fluids and Structures 23 pp. 429-445
[10] Kuiper G.L., and Metrikine A.V., 2008, "Experimental investigation of dynamic stability of a cantilever pipe aspirating fluid," J. of Fluids and Structures 24 pp. 541-558
[11] Giacobbi, D.B., 2007 A numerical and experimental study of the dynamics of aspirating cantilever pipes. Undergraduate honours thesis, Department of Mechanical Engineering, McGill University, Montreal, Canada.
[12] Giacobbi, D.B., Semler, C. and Païdoussis, M.P. 2008, "Numerical Fluid-Structure Interaction Study of a Cantilevered Pipe Discharging or Aspirating Fluid via a Computational Fluid Dynamics and Finite Element Analysis Model", in Proceeding of the Sixth International Conference on Engineering Computational Technology, Athenes M. Papadrakakis & B.H.V Topping eds. Paper 48, pp 1-18
[13] Done, G.T.S., and Simpson A., 1977, "Dynamic instability of certain conservative and non-conservative systems," J. Mec. Eng. Science 19 (6) pp. 251-263
[14] Païdoussis, M.P., and Issid, N.T., 1974, "Dynamic stability of pipes conveying fluid," J. of Sound and Vibration 33 pp. 267-294
[15] Bisplinghoff, R.L., Ashley, H. and Halfman, R. L. Aeroelasticity, 1996 Dover edition corrected republication of the first publication in 1955 by Addison-Wesley Publishing Company Cambridge Massachussets, U.S.A ,Chap. 1.
[16] Blevins, R.D., 1992, Applied Fluid Dynamics Handbook. Krieger Publishing Company Malabar, Florida Chap. 5.
[17] Idel'cik, I.E., 1960, Memento des pertes de charge (French translation from the Russian, 1969), *Eyrolles*, Paris, France.
[18] Feynmann R.P., 1985, Surely You're Jocking Mr Feynmann. Norton New-York pp. 63-65.
[19] Forrester, T., 1986, "Inverse sprinklers: A lesson in the use of conservation principle," Am. J. of Physics 54 (9) pp. 798-800
[20] Wheeler, J.A., 1989, "The young Feynman," Physics Today pp. 24-28
[21] Weyland, J.A., and Patterson, J.D., 1976 "Rotating water sprinkler," Am. J; of Physics 44, (11) pp. 1106-1109
[22] Berg, R.E., and Collier M.R., 1989, "The Feynman inverse sprinkler problem: A demonstration and quantitative analysis," Am. J. of Physics 57 (7) pp. 654-657
[23] Collier, M.R., Berg, R. E., and Ferrell R.A., 1990, "The Feynman inverse sprinkler problem: a detailed kinematic study," Am.J.Phys 59 (4) pp. 349-355
[24] Païdoussis, M.P., and Tétreault-Friend, M., 2009, "Aspirating cantilevers and reverse sprinklers," Am. J. Phys. 77 (4) pp. 349-353
[25] Pramila, A., 1992, "Undamped cantilever aspirating fluid may be stable". Rakenteiden Mekaniikka 25, pp. 3-14
[26] Benjamin, T.B., 1961, "Dynamics of a system of articulated pipes conveying fluid: 1 Theory". Proc. R. Soc. London, Ser. A 261, pp. 457-486
[27] Benjamin T.B., 1961b, "Dynamics of a system of articulated pipes conveying fluid: 2 Experiments" Proc. R. Soc. London, Ser. A 261, pp. 487-499.
[28] Lindgren, E.R., 1990, "The transport of momentum theorem" Am. J. of Physics 58, (4) pp. 352-357
[29] Axisa, F. Antunes, J. 2007, Modelling of mechanical systems. Volume 3 Fluid-Structure Interaction, Chap. 6. Elsevier, London.

